Nonadiabatic effects on peptide vibrational dynamics induced by conformational changes

Jens Antony, Burkhard Schmidt,[a] and Christof Schütte
Freie Universität Berlin, Institut für Mathematik II, Arnimallee 2–6, D-14195 Berlin, Germany

(Received 29 September 2004; accepted 14 October 2004; published online 14 December 2004)

Quantum dynamical simulations of vibrational spectroscopy have been carried out for glycine dipeptide ($CH_3-CO-NH-CH_2-CO-NH-CH_3$). Conformational structure and dynamics are modeled in terms of the two Ramachandran dihedral angles of the molecular backbone. Potential energy surfaces and harmonic frequencies are obtained from electronic structure calculations at the density functional theory (DFT) [B3LYP/6-31+G(d)] level. The ordering of the energetically most stable isomers (C_7 and C_5) is reversed upon inclusion of the quantum mechanical zero point vibrational energy. Vibrational spectra of various isomers show distinct differences, mainly in the region of the amide modes, thereby relating conformational structures and vibrational spectra. Conformational dynamics is modeled by propagation of quantum mechanical wave packets. Assuming a directed energy transfer to the torsional degrees of freedom, transitions between the C_7 and C_5 minimum energy structures occur on a sub-picosecond time scale (700···800 fs). Vibrationally nonadiabatic effects are investigated for the case of the coupled, fundamentally excited amide I states. Using a two state-two mode model, the resulting wave packet dynamics is found to be strongly nonadiabatic due to the presence of a seam of the two potential energy surfaces. Initially prepared adiabatic vibrational states decay upon conformational change on a time scale of 200···500 fs with population transfer of more than 50% between the coupled amide I states. Also the vibrational energy transport between localized (excitonic) amide I vibrational states is strongly influenced by torsional dynamics of the molecular backbone where both enhanced and reduced decay rates are found. All these observations should allow the detection of conformational changes by means of time-dependent vibrational spectroscopy. © *2005 American Institute of Physics.*
[DOI: 10.1063/1.1829057]

I. INTRODUCTION

Conformational structure and dynamics of peptides and proteins are of fundamental importance in molecular biology; in particular the three-dimensional structure of peptide chains determines their biological function, e.g., their role in storing and transporting energy. One way to explore conformations of biopolymers is provided through vibrational spectroscopy.[1–3] In the last few years, the field has strongly benefitted from the development of nonlinear two-dimensional, transient spectroscopy[4–8] and from the use of sophisticated double-resonance techniques.[9–11] The latter allow to measure vibrational spectra in the molecular fingerprint region for selected conformations only. Thus, vibrational spectroscopy has become instrumental in establishing a relation between the (infrared) spectrum and the (peptide backbone) conformational structure of simple amino acids and dipeptides where the assignment of conformers is partly aided by DFT calculations. There is also remarkable progress on the investigation of conformational dynamics: Time-dependent two-dimensional vibrational spectroscopy, often in connection with simulation studies, allows to learn about the flexibility inside conformations through observation of sub-picosecond fluctuations.[12–14] Under favorable circumstances, also conformational isomerization dynamics can be observed by means of transient spectroscopy on a picosecond timescale. So far this concept has been realized either by integrating a photo-switch into the backbone of a cyclopeptide[15] or by selective infrared excitation of a dipeptide.[16] Further development of the latter technique has also led to direct measurement of energetic thresholds to conformational changes.[17]

Many of the above-mentioned studies of conformational structure and dynamics rely on spectroscopy of the amide vibrational modes, which are essentially localized within the peptide bonds (–CO–NH–). In a dipeptide the corresponding vibrational frequencies occur in pairs where the splittings reflect both the different local environment of the individual peptide units as well as the interaction among them. Being very sensitive to the distance and relative orientation between different peptide units, they provide valuable information on the (secondary) structure of peptides or proteins.[18–21] In particular, the amide I modes which mainly consist of CO stretching vibrational motions are frequently used in studies of conformational structure because there is essentially no intramolecular coupling between the amide I mode and other internal modes.[22] Although the main mechanism that couples amide I vibrations of different peptide units can be assigned to the interaction of transition dipoles (''through space''),[1] recent studies have revealed the importance of subtle

[a]Electronic mail: burkhard@math.fu-berlin.de

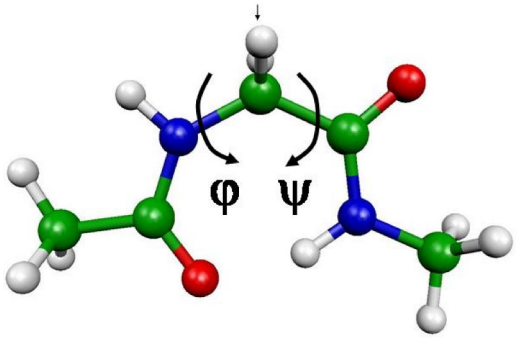

FIG. 1. (Color online) Reduced model for conformational dynamics of GLD defining the Ramachandran angles (here $\phi=\psi=0$). All other degrees of freedom are assumed to be fixed.

changes of the electronic charge distribution (''through bond'').[23,24]

Almost all theoretical work on molecular dynamics of peptides and proteins is based on the classical approximation, thereby neglecting any kind of quantum effects. However, there are a few noteworthy exceptions in the literature where quantum effects on vibrational spectroscopy of biomolecules are pioneered: The effect of anharmonic coupling and zero point vibrational energy has been explored for peptides[22,25] and even proteins.[26,27] Other workers have modeled energy transfer in collisions of solvent particles with peptides[28–30] and proteins[31] by means of (partly) quantum-dynamical methods. These studies are based on the adiabatic (Born–Oppenheimer) approximation, i.e., the movement of the atoms is dictated by a single potential energy hypersurface, usually that of the electronic ground state. This is justified by the discrepancy of time scales of fast (electronic) and slow (nuclear) degrees of freedom. It is very suggestive to apply this approach to the separation of fast and slow vibrational modes as well. In the present study we shall use the separation of (fast) bond stretching and (slow) torsional motions of a model peptide system. In particular, the dependence of amide *I* vibrationally excited state dynamics on conformational structure and dynamics shall be investigated. In this context deviations from purely adiabatic behavior are very intriguing. The study of nonadiabatic effects, originally established in the realm of classical mechanics[32,33] has been adapted in recent years to the field of quantum molecular dynamics.[34,35] In vibronic dynamics the extreme mass ratio of electrons (m) versus nuclei (M) leads to a nonadiabaticity parameter of $\epsilon=\sqrt{m/M}\approx 10^{-2}$. This essentially limits the importance of nonadiabatic effects to the regions of seams or conical intersections of potential energy surfaces. In contrast, for vibrationally nonadiabatic dynamics this parameter is less extreme with $\epsilon\approx 10^{-1}$ suggesting an even more important role of nonadiabatic effects induced by conformational dynamics.

The present study is on the simplest model for the interaction of two adjacent peptide fragments in a polypeptide chain without side chains, i.e., glycine dipeptide (GLD, $CH_3-CO-NH-CH_2-CO-NH-CH_3$), see Fig. 1. While solvent effects undoubtedly have important influence on the conformations of biopolymers, we restrict ourselves to the dipeptide dynamics *in vacuo*. Elimination of intermolecular influences allows to study only intramolecular effects on biomolecular conformation.[9] Another advantage of studying biomolecules in the gas phase lies in the reduced numerical effort of computational studies: While simulations of peptides in solution are up to date restricted to classical simulations based on (semi-) empirical force fields, electronic structure calculations of smaller peptide chains *in vacuo* are now routinely carried out. This includes both density functional theory (DFT) and Hartree–Fock based methods, in some cases using high-level theory to account for electronic correlation.[36–39] At the same time, it allows to study quantum effects on molecular dynamics by means of wavepacket dynamics. Hence, the present study of glycine dipeptide can be regarded as a benchmark where the importance of quantum effects shall be demonstrated and where the adequacy of the approximations typically used in simulations of larger systems can be critically evaluated. Our specific emphasis is on the importance of nonadiabatic effects on the dynamics of vibrationally excited states. This is motivated by the previous finding of seams of the potential energy surfaces giving the torsional dependence of amide *I* excited states.[19] of GLD *in vacuo*. In addition to the relation between conformational structure and vibrational spectrum, the main focus is on how conformational dynamics manifests itself in vibrationally nonadiabatic effects. This should eventually open new ways to the identification of conformational changes using transient vibrational spectroscopy. The remainder of the paper is organized as follows: In Sec. II we develop a reduced dipeptide model together with a Hamiltonian describing the vibrationally nonadiabatic quantum dynamics. In Sec. III we present our results for potential energy surfaces and wavepacket dynamics describing conformational structure and changes. Our conclusions can be found in Sec. IV.

II. MODEL HAMILTONIAN

A. Reduced dipeptide model

In the present work we investigate the quantum dynamics of glycine dipeptide (GLD, $CH_3-CO-NH-CH_2-CO-NH-CH_3$). The essential degrees of freedom are the torsional rotations of the individual peptide units ($-CO-NH-$) about the backbone of the chain, where ϕ and ψ describe the torsion of the N-terminus ($CH_3-CO-NH-$) and the C-terminus ($-CO-NH-CH_3$), respectively, with regard to the central CH_2 group, see Fig. 1. The plane spanned by the two angles (ϕ,ψ) is referred to as Ramachandran surface[40] with values of $(\pm 180°, \pm 180°)$ corresponding to a fully extended conformation of the chain.[41] For long polypeptide chains these angles serve to characterize typical secondary structural motifs such as helices and sheets. We assume the remaining degrees of freedom to follow the torsional dynamics in an adiabatic manner. This is realized by minimizing the potential energy for each given (ϕ,ψ) pair (see Sec. II B) whereas the construction of the kinetic energy operator fixes the other degrees of freedom to their average over the Ramachandran plane (see Sec. II C). While the variations of bond lengths and bond angles are known to be

negligible, minor deviations from planarity of the peptide bonds exist, see recent studies of N-methylacetamid (NMA, $CH_3-CO-NH-CH_3$)[38] and GLD.[36]

B. Potential energy surface

Density functional theory (DFT) has proven to be a powerful method for the calculation of electronic structure of molecular systems.[42] In recent years this method has been well established for biologically relevant systems. For the NMA molecule, comparison of various nonlocal methods yields good agreement with Hartree–Fock calculations including second-order Møller–Plesset (MP2) corrections for the conformational structure, torsional barriers, and vibrational frequencies.[38] Similarly encouraging findings were made for GLD[20] as well as for alanine dipeptide.[36,39]

In the present investigation of neutral glycine dipeptide in vacuum all electron structure calculations were performed using the DFT implementation of GAUSSIAN 98.[43] The combination of the 6-31+G(d) split-valence polarized basis set including diffuse functions with the B3LYP hybrid functional is known to provide good overall agreement of calculated normal mode vibrational frequencies with experimental data. In order to study the torsional dependence of potential energy and vibrational frequencies, the Ramachandran plane is scanned with a step size of 10°. Accounting for the symmetry with respect to inversion through the origin (0°,0°), this amounts to a total of 667 independent points. For each point a partial geometry optimization was carried out, i.e., all degrees of freedom except (ϕ,ψ) were fully relaxed. The harmonic frequencies resulting from a vibrational normal mode analysis were scaled with a factor 0.96 to account for higher electronic correlations and vibrational anharmonicity, which is the recommended scaling factor for B3LYP/6-31G(d) level of theory.

C. Nonadiabatic Hamiltonian

The construction of an exact kinetic operator for the study of vibrations and rotations in terms of curvilinear coordinates is a nontrivial task. In the reduced dynamical model of the present work (Sec. II A), there are only two active degrees of freedom $q=(\phi,\psi)^T$ while all other degrees of freedom are kept frozen. We follow the approach outlined in Refs. 44–46 which is tailored to the case of rather few active degrees of freedom in highly constrained systems. Eliminating the contributions of external molecular translation and rotation and setting the total angular momentum to zero, the kinetic energy can be expressed as

$$T_{\mathrm{vib}}=\tfrac{1}{2}p^T\mathbf{G}(q)p, \tag{2.1}$$

where p stands for the vector of momenta conjugate to q and where $\mathbf{G}$ is the metric tensor for the (two) active degrees of freedom only.[46] Neglecting the relaxation of the remaining degrees of freedom, this expression is transformed to a quantum mechanical one by replacing p with $-i\hbar\nabla$. In order to describe the dynamics of vibrationally excited states of the dipeptide amide vibrations, the following diabatic representation of the (matrix-valued) Hamiltonian is used:

$$H(q)=V(q)-\frac{\hbar^2}{2}\nabla_q^T\mathbf{G}(q)\nabla_q 1, \tag{2.2}$$

where V stands for the (symmetric) potential energy matrix and 1 stands for the unit matrix. Although standard quantum chemical software yields adiabatic potential energy surfaces, the problem of sharply peaked or even singular nonadiabatic coupling functions is circumvented by the choice of a diabatic basis. Finding such a transformation is highly nontrivial or—in the multidimensional case—even impossible.[47] However, for the two state-two mode model considered in the present study, it does not present a special difficulty. The upper (+) and lower (−) adiabatic states, $|u_i(q)\rangle$, can be written as linear combinations of two diabatic (q-independent) basis states

$$\begin{aligned}|u_+(q)\rangle&=\sin\alpha(q)|u_1\rangle+\cos\alpha(q)|u_2\rangle,\\ |u_-(q)\rangle&=\cos\alpha(q)|u_1\rangle-\sin\alpha(q)|u_2\rangle,\end{aligned} \tag{2.3}$$

where α is referred to as mixing angle. Although the (symmetric) potential energy matrix V contains off-diagonal contributions, the numerical advantage over the use of an adiabatic representation stems from the fact that these functions are generally much smoother in q. To facilitate interpretation of the results, it is convenient to transform the results to the adiabatic representation.

The numerical treatment rests on fast Fourier transform methods for the transformation between coordinate and momentum space. Wave functions are represented on an equidistant grid in coordinate space[48] comprising of 256×256 points in $[-\pi,\pi[^2$ employing periodic boundary conditions. The time-independent Schrödinger equation is solved by propagation in imaginary time.[49] Solution of the time-dependent Schrödinger equation is achieved by the $\mathcal{O}(\Delta t^3)$ Strang splitting technique[50] with extension to coupled states.[51]

III. RESULTS AND DISCUSSION

A. Ground state surface

The potential energy surface of GLD *in vacuo* was generated by DFT calculations at the B3LYP/6-31+G(d) level of theory, for details see Sec. II B. The stationary points are listed in Table I with the minima illustrated in Fig. 2. The energetically lower portions of the potential energy surface can be found near the diagonal $\phi=-\psi$ which corresponds to an anti-geared rotation of the two peptide units around the central CH_2 group, see Fig. 3. The global minimum (C_7) is found at $(\phi,\psi)=(-82°,69°)$. Next there is a local minimum at $(\pm180°,\pm180°)$ corresponding to the planar, fully extended C_5 conformation which is 2.1 kJ/mol higher in energy. Note that both these structures are energetically favorable due to the formation of seven- and five-ringlike structures closed by (strongly) frustrated intramolecular hydrogen bonds.[36] They are separated by a barrier of appreciable height (7.7 kJ/mol). Finally there is a much higher saddle (31.9 kJ/mol) at the inversion center (0°,0°) separating the two (symmetry-equivalent) C_7 minima. There is yet another, rather shallow, local minimum at (−113°,17°) which can be assigned to a β-like conformation (9.3 kJ/mol). However, the

TABLE I. Stationary points (ϕ, ψ in degrees), potential energies and zero point energies (in kJ/mol) for GLD *in vacuo* obtained from DFT calculations [B3LYP/6-31+G(d)].

	ϕ	ψ	E	ΔE
C_7	−82.1	69.1	0.00[a]	417.07
C_5	−180.0	179.9	2.14	414.60
$C_7 \leftrightarrow C_5$	−98.2	128.3	7.73	415.99
β	−112.8	17.2	9.29	415.44
$\beta \leftrightarrow C_7$	−104.9	24.6	9.49	415.03
$\beta \overset{\leftrightarrow}{_{\text{alt}}} C_7$	−113.7	19.8	10.00	415.20
Cusp	180.0[b]	0.0[b]	27.39	415.97
$C_7 \leftrightarrow C_7$	0.0	0.0	31.88	417.07
$\beta \leftrightarrow \beta$	−112.9	−56.6	33.64	413.49
$C_7 \overset{\leftrightarrow}{_{\text{alt}}} C_7$	3.0	80.4	42.44	415.25
Max	0.0[b]	180.0[b]	94.00	413.05

[a]The zero of energy is $-456.5609 E_h$.
[b]Restrained values.

transition to the C_7 structure is not very pronounced. Other important features of the potential energy surface are the distinct maxima at $(0°, \pm 180°)$ and at $(\pm 180°, 0°)$ reflecting the steric hinderance of the carbonyl oxygen atoms and the amide hydrogen atoms, respectively.

Upon generating the Ramachandran plot of Fig. 3, the remaining degrees of freedom were relaxed. The resulting standard deviations of bond lengths for the backbone atoms are less than 1 pm while those of valence angles reach up to 4° for the case of the central N–C–C angle. The ω torsion angles of the two peptide bonds have standard deviations of

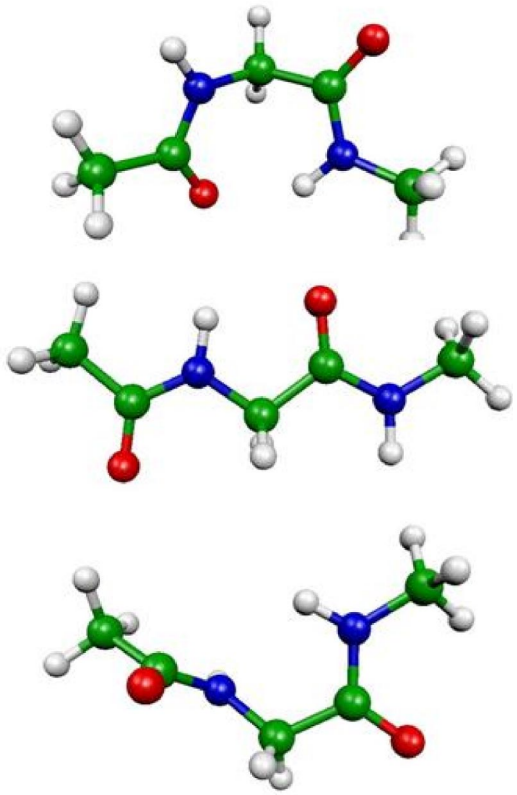

FIG. 2. (Color online) Energetically lowest conformations of GLD *in vacuo*. From top to bottom C_7 $(-82°,69°)$, C_5 $(180°,180°)$, β $(-113°,17°)$.

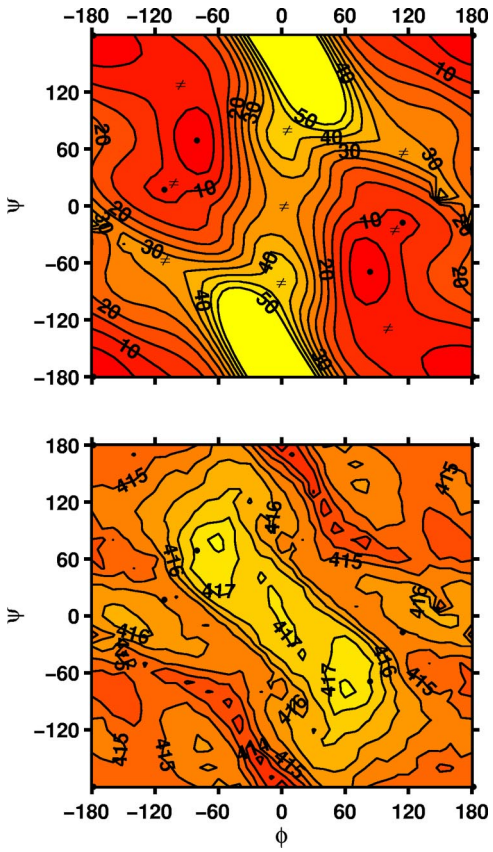

FIG. 3. (Color online) Results of DFT calculations for GLD *in vacuo* [B3LYP/6-31+G(d)]. Upper figure: Potential energy (in kJ/mol). Contours at energies above 50 kJ/mol are omitted. Lower figure: Zero point vibrational energy (in kJ/mol). Minima and saddle points of the potential (see Table I) are marked by filled circles (●) or by transition state symbols (≠), respectively.

15° and 4° and deviate maximally by ±41° and ±9° from planarity for the N- and C-terminal peptide bond, respectively. However, the rather large values for the N-terminal peptide bond occur in the energetically unfavorable regions around $(0°, \pm 180°)$ and $(\pm 180°, 0°)$, while the deviation from planarity in the relevant part of the Ramachandran plane is only around 10°. The standard deviations of the rotational constants of the reduced model and the relaxed geometries amount to 9, 15, and 14%, for the smallest, medium, and largest moment of inertia, respectively. Again, the largest deviations are found in energetically high-lying regions of the Ramachandran plane. In summary, these observations strongly support the reduced model of Sec. II A used throughout the remainder of this work.

Although the main qualitative features of the potential energy surfaces are rather similar, a quantitative comparison with the results of previously published electron structure calculations is intriguing: Using a relatively small basis set (3-21G), 11 independent stationary points were identified which reduce to 7 points when increasing the basis size to 6−31+G(d) for a glycine dipeptide analogue (replacing terminal methyl groups by hydrogen atoms) using Hartree–Fock (HF) based calculations,[36] see also Table I. The HF energy difference between the C_7 and C_5 minima has about the same magnitude as the present B3LYP result but opposite

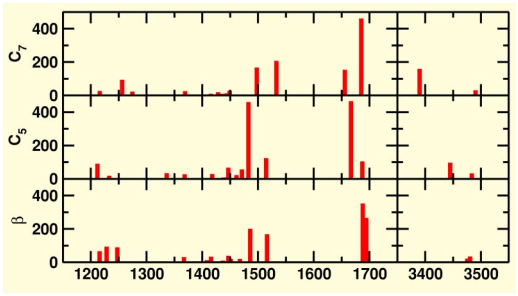

FIG. 4. (Color online) Infrared spectra of GLD from DFT calculations [B3LYP/6-31+G(d)]. The figure shows scaled (0.96) harmonic frequencies (in cm^{-1}) and intensities (in km/mol) for three minimum energy configurations, see also Table I.

sign. However, when including electron correlation at the MP2 level the energetic order of C_7 and C_5 is reversed but the energetic spacing is about twice as large as in our DFT results. While the energies of the $C_7 \leftrightarrow C_5$ transition states are similar in all three methods, our B3LYP result for the $C_7 \leftrightarrow C_7$ structure is more than 6 kJ/mol lower than the MP2//HF result of Ref. 36. Other calculations at the restricted HF level employing a larger basis set [6-311++G(d,p)] report the same ordering of the minima and similar spacing as well as similar difference between the energetically lowest and highest structures.[19] In passing we also note recent work on alanine dipeptide where a similar trend has been found in a comprehensive comparison of quantum-chemical methods: When increasing the level of theory, the potential energy surface is becoming smoother which may lead to a decrease of the number of local extrema.[39]

B. Vibrational analysis

A vibrational analysis for each pair of torsional angles (ϕ,ψ) has been carried out as described in Sec. II B. This immediately allows to calculate the torsional dependence of the zero point energy, ΔE, associated with the remaining (fast) degrees of freedom. In the context of the vibrationally adiabatic approximation, the ground adiabatic potential energy surface, $E_0 = E + \Delta E$, for the slow (torsional) coordinates is obtained by adding ΔE to the electronic potential energy surface E. The zero point energy varies by more than 4 kJ/mol within the Ramachandran plane. It exhibits a global maximum and a local minimum near the C_7 and C_5 conformation, respectively. Thus, inclusion of the zero point effect reverses the energetic ordering of the minima rendering the C_5 to be 0.3 kJ/mol more stable than the C_7 structure, see also Table I and the lower panel of Fig. 3. Note that this behavior cannot be assigned to one (or a few) normal modes only but it rather involves almost all vibrational modes.

Typical results of the harmonic vibrational analysis can be seen in Fig. 4 where scaled harmonic frequencies and corresponding infrared intensities are displayed for the three minima (C_7, C_5, β) of the potential energy surface. Our emphasis is on the amide vibrational modes which are essentially localized within the (planar) peptide bonds (CO–NH). In a dipeptide these modes become—to a certain extent—delocalized giving rise to close-lying pairs of spectral lines corresponding to symmetric or anti-symmetric combinations of the individual peptide vibrations. The infrared spectra for the three isomers of glycine dipeptide exhibit significant differences both in frequencies and intensities: There are strong changes not only for the amide *A* mode (NH stretching, $3400\cdots3500\ cm^{-1}$) but also for the modes involving movement of the heavier atoms: Those include the amide *I* mode (mainly CO stretching, $1650\cdots1700\ cm^{-1}$), the amide *II* and *III* modes (CN stretching and NH bending, $1450\cdots1550\ cm^{-1}$ and $1200\cdots1300\ cm^{-1}$, respectively). The amide *I* modes present an especially interesting case: The higher infrared absorbance indicates that the upper amide *I* mode of the C_7 conformation is mainly antisymmetric and its frequency exceeds that of the lower one by $31\ cm^{-1}$. This ordering is reversed for the C_5 conformation where the frequency splitting is $21\ cm^{-1}$.

C. Normal modes of amide *I* vibration

In the following we study the torsional dependence of the normal mode frequencies. In doing so, we shall restrict ourselves to the investigation of the amide *I* modes. Because of the high infrared intensity, the relatively isolated frequency and the conformational sensitivity (see Fig. 4) they are most frequently studied in spectroscopic experiments.[2,3] Furthermore, anharmonic vibrational analysis of NMA has revealed that there is essentially no intramolecular coupling between the amide *I* mode and other internal modes[22] although some coupling to the amide *A* mode has been detected in a recent study of model peptides.[52] The combinations of the two local peptide vibrations shall be denoted as ω_+ and ω_- for the upper and lower combination, respectively. The center frequency $(\omega_+ + \omega_-)/2$ varies between 1668 and $1733\ cm^{-1}$, see upper panel of Fig. 5. The overall shape of the surface is similar to that of the potential energy, i.e., the minima are lying on the diagonal $\phi = -\psi$ at $(-50°,50°)$ and $(50°,-50°)$, with a local minimum at the fully extended structure $(180°,180°)$. These minima are mainly due to the intramolecular hydrogen bonds occurring in these structures, which are known to lower the amide *I* frequencies by $20–25\ cm^{-1}$ for hydrogen bonds to the C═O group and by $10–20\ cm^{-1}$ for hydrogen bonds to the NH group.[3] The maximum center frequency is found at $(0°,\pm180°)$ reflecting the repulsion of the carbonyl oxygen atoms.

The variation of the splitting of the two amide *I* mode vibrational frequencies, $\omega_+ - \omega_-$, can be seen in the middle part of Fig. 5. A steep-walled plateau encompasses the two equivalent C_7 structures and the $C_7 \leftrightarrow C_7$ transition structure $(0°,0°)$. Another local maximum is the C_5 conformation at $(\pm180°,\pm180°)$. These results closely resemble the HF/6-311++G(d,p) frequencies of glycine dipeptide presented in Ref. 19. However, our DFT center frequencies are shifted by about $30\ cm^{-1}$ to lower values compared to the HF ones, and the range of variation of the difference frequency is slightly smaller for the DFT calculation than for HF.

Within the framework of the two state–two mode model introduced in Sec. II C, i.e., assuming that the (coupled) amide *I* modes are decoupled from the remaining vibrations

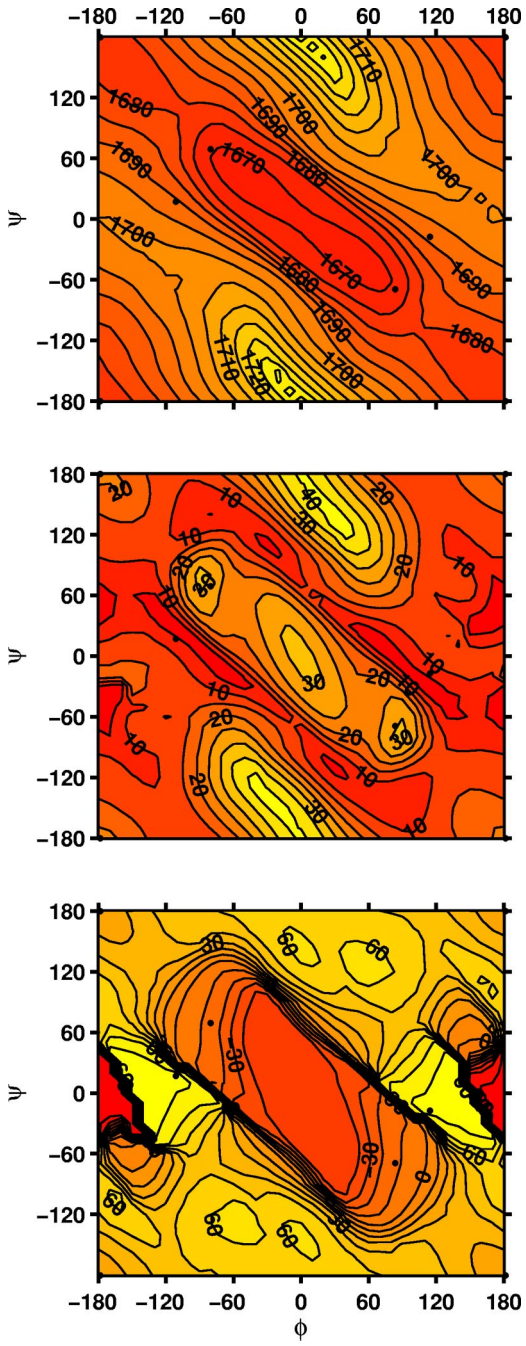

FIG. 5. (Color online) Normal mode frequencies of GLD fundamental amide *I* vibrational excitation. Top to bottom: Center frequency $(\omega_+ + \omega_-)/2$ (in cm^{-1}), difference frequency $\omega_+ - \omega_-$ (in cm^{-1}), mixing angle α (in degrees). Minima of the potential energy surface are marked by filled circles (●), see also Fig. 3.

of glycine dipeptide, the amide *I* normal modes can be expressed as linear combinations of amide *I* vibrations localized in the N-terminus, $|u_1\rangle$, or in the C-terminus, $|u_2\rangle$. In practice, the mixing angle α (2.3) is determined from the structure of the normal modes considering the ratio of the displacements of the C═O groups in the upper amide *I* normal mode from their equilibrium positions.[21,23] This ratio was also taken for the lower amide *I* mode. Indeed, the deviations were on the average about 3%. As a further consistency check, the displacements of N and H atoms were also investigated. However, there the mean deviations were 33% and 47% for N and H, respectively, which indicates the non-negligible admixture of other vibrational modes, mainly the amide *A* mode, see also.[52]

The mixing angle has a trough region containing the two C_7 structures and the transition state (0°,0°), where it has values down to −45°, corresponding to delocalized normal modes, see lower part of Fig. 5. Together with the information on the difference frequency we conclude that in this region of the Ramachandran plane the frequency of the symmetric amide *I* mode is significantly lower than the antisymmetric one. The mixing angle abruptly changes sign at the walls of the trough and varies between 20° and 60° outside, corresponding again to fairly delocalized normal modes but where the symmetric frequency is higher than the antisymmetric one. An exception is the region around (±180°,0°), where its absolute value is close to 90°, i.e., localized amide *I* vibrations. In conclusion, there is evidence for the existence of a seam of the two vibrationally adiabatic surfaces at the walls of the plateau thus separating the C_7 and C_5 conformer. This is of key importance for the non-adiabatic quantum dynamical studies of Sec. III F. Note that on the basis of our relatively coarse meshed potential surfaces it is impossible to distinguish between a true or an avoided intersection. However, in a study of nonadiabatic photo-reactions it has been shown that the exact topology of the crossing surface does not influence the resulting population dynamics for the case of nondissipative wave packet propagation.[53]

It is intriguing to investigate how the amide *I* normal mode frequencies are changed by anharmonic effects. For the most important stationary points of glycine dipeptide, potential energies are calculated with the above described DFT technique in the plane spanned by the two amide *I* normal coordinates. The magnitude of the resulting diagonal and off-diagonal anharmonic constants is between 2 and $4\ \mathrm{cm}^{-1}$ only. For comparison, we calculated a value of $4\ \mathrm{cm}^{-1}$ for the amide *I* frequency of a single peptide unit in NMA. In the absence of experimental results for peptide systems *in vacuo*, we note that this value is twice as large for solvated systems.[4] The overall effect of the anharmonicity is that the amide *I* frequencies for the three minima (C_7, C_5, β), the connecting transition states, and the local maxima are all reduced by $8\ \mathrm{cm}^{-1}$ while the frequency differences are hardly affected.

D. Local modes of amide *I* vibration

With the mixing angle α of Eq. (2.3) and the two amide *I* normal mode frequencies, ω_+ and ω_-, available, it is straightforward to reconstruct the amide *I* vibrational Hamiltonian in the basis of the two localized (excitonic) amide *I* vibrations (2.2) where $V_{11}=E_0+\hbar\omega_1$ and $V_{22}=E_0+\hbar\omega_2$ are the potential energy surfaces corresponding to local amide vibrational excitations of the N- and C-terminus, respectively. The resulting difference of the local frequencies[20,23]

$$\omega_2-\omega_1=(\omega_+-\omega_-)\cos(2\alpha), \tag{3.1}$$

is displayed in the upper part of Fig. 6. In contrast to the adiabatic frequency difference $\omega_+-\omega_-$, which is also influenced by the inter-peptide coupling discussed below, the di-

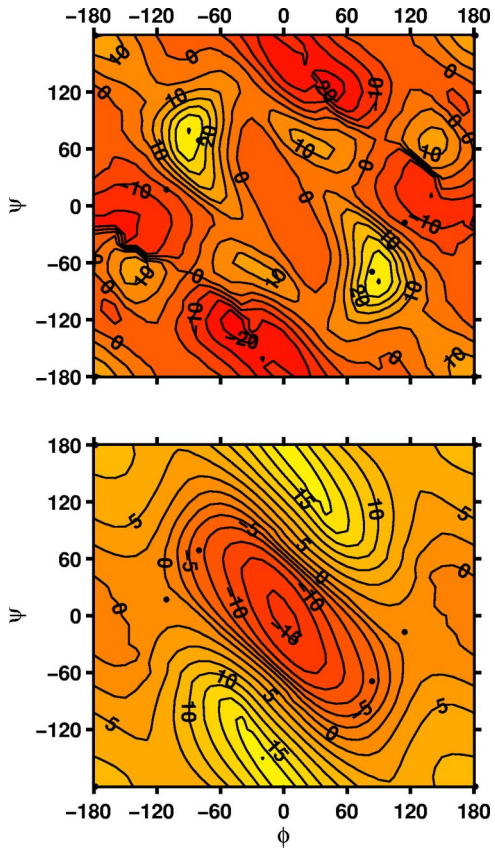

FIG. 6. (Color online) Local mode frequencies of GLD fundamental amide *I* vibrational excitation. Top: Difference of local amide *I* frequencies of N-terminus and C-terminus (in cm^{-1}). Bottom: Inter–peptide coupling parameter V_{12} (in cm^{-1}). Minima of the potential energy surface are marked by filled circles (●), see Fig. 3.

abatic frequency gap varies less than the adiabatic one and reflects changes in hydrogen bonding and steric hinderance as a function of the backbone conformation. The global maxima ($30.4\ cm^{-1}$) close to the C_7 structures are characterized by the inter-peptide hydrogen bond of the C_7 structure between the CO group of the N-terminal and the NH group of the C-terminal peptide unit. Since the amide *I* frequency is affected more by a hydrogen bond to the CO than to the NH group,[3] ω_1 is reduced more than ω_2, leading to a positive frequency difference. At the local maximum ($12.5\ cm^{-1}$) for the C_5 structure the NH bending contribution of the amide *I* mode on the N terminus is more perturbed than the CO stretching on the C terminus, and again ω_1 is reduced more than ω_2, but to a lesser extend than in the C_7 structure. The minima close to $(0°,\pm 180°)$ and $(\pm 180°,0°)$ are characterized by steric contacts between the peptide CO groups and the peptide NH groups, respectively, which tends to increase the vibrational frequency. Again it is the amide *I* mode on the N terminus that is affected more than that on the C terminus, resulting in negative diabatic frequency differences.

Also the inter-peptide coupling can be deduced from the normal mode frequencies and structure given in Sec. III C. The off-diagonal element of Hamiltonian (2.2) can be written as[20,23]

$$V_{12} = \hbar(\omega_+ - \omega_-)\sin(2\alpha)/2. \tag{3.2}$$

The lower panel of Fig. 6 shows a wide region with negative coupling in the center of the Ramachandran plane with the minimum at the inversion center of the molecule, $(0°,0°)$ while the global maximum is found at $(0°,\pm 180°)$. The minimum energy conformations C_7 and C_5 are located at either side of the zero line with a coupling value of -6.5 and $8.0\ cm^{-1}$, respectively.

Our results for the inter-peptide coupling are essentially identical to those obtained from HF/6-311++G(*d*,*p*) calculation, see Ref. 20, so that accounting for electronic correlation in our DFT calculations appears not to alter the result for this quantity, which was also noted in Ref. 23 where results of a partial *ab initio* calculation using B3LYP/6-31+G(*d*) are compared with the HF/6-31(+)G(*d*,*p*) results of Ref. 18. Note that all of the mentioned electronic structure calculations differ qualitatively from results obtained from the semiempirical transition dipole coupling (''through space'') which has been widely used to calculate amide *I* spectra of polypeptides or even proteins.[1–3] The pronounced trough in the center of the Ramachandran plane does not exist in calculations of the dipole–dipole interaction. Apparently, this shortcoming is due to the neglect of charge flows along the peptide chain (''through bond'').

E. Adiabatic conformational dynamics

In this section we study the quantum dynamics of conformational transitions of glycine dipeptide. As a first step we have to evaluate the kinetic energy operator (2.1) for the highly constrained model of dipeptide dynamics. For the case of uncoupled internal motions, the rotational constants would be $0.1442\ cm^{-1}$ for the N-terminus (CH_3–CO–NH–) and $0.2221\ cm^{-1}$ for the C-terminus (–CO–NH–CH_3). Because the axes of internal rotation do not coincide with the corresponding principle axes of the tensors of inertia, the internal rotations couple to the center of mass translation and to the external rotation. Elimination of these effects leads to[46]

$$\frac{h\mathbf{G}}{8\pi^2 c} = \begin{pmatrix} 0.2144 & -0.0250 \\ -0.0250 & 0.2888 \end{pmatrix} \pm \begin{pmatrix} 0.0073 & 0.0139 \\ 0.0139 & 0.0126 \end{pmatrix}, \tag{3.3}$$

where mean values and standard deviations are given in wave number units (cm^{-1}), see also Fig. 7. Throughout the remainder of this work, we shall neglect the relatively weak (ϕ,ψ) dependence of the **G**-tensor and replace its elements by their mean values which simplifies evaluation of the quantum kinetic operator. This is well justified for the diagonal elements where the standard deviation is below 5% of the mean value. Although the off-diagonal element varies appreciably, its magnitude is so small that even neglecting $G_{\phi\psi}$ altogether leads only to minor deviations of the simulation results presented below. Moreover, for longer peptide chains or even proteins the interaction of the torsional modes with the overall rotation and translation becomes negligible since the rotational constants of the molecule are very small.[27,54]

In a first set of simulations we investigate the torsional dynamics of the molecule in the amide *I* vibrational ground

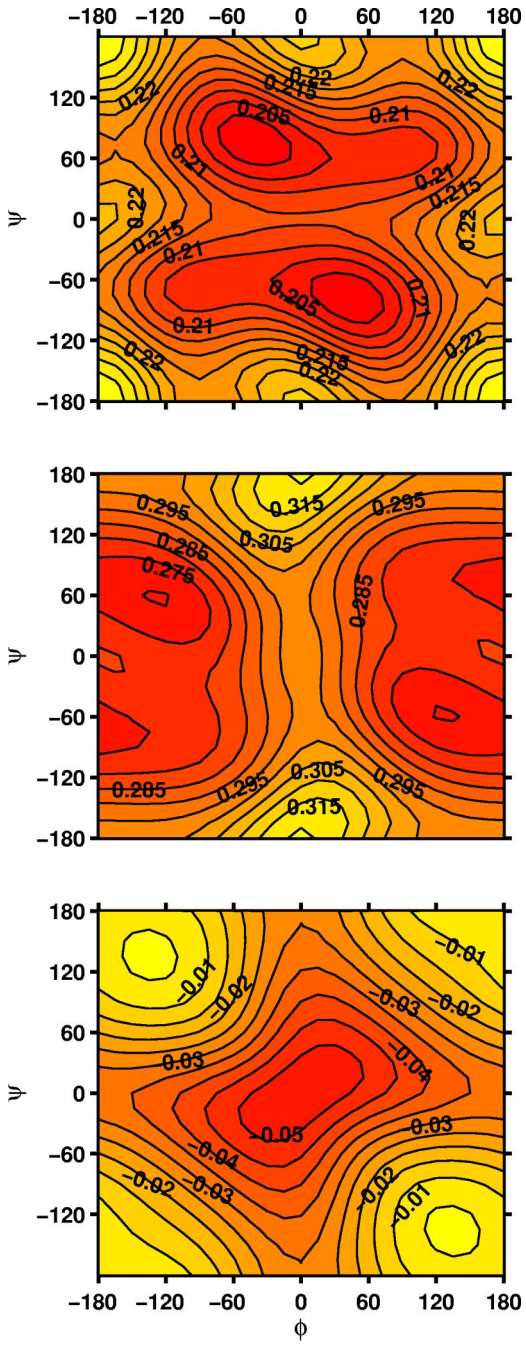

FIG. 7. (Color online) **G**-tensor elements for reduced model of GLD. From top to bottom: $hG_{\phi,\phi}/(8\pi^2 c)$, $hG_{\psi,\psi}/(8\pi^2 c)$, $hG_{\phi,\psi}/(8\pi^2 c)$, in units of wave numbers (cm^{-1}).

state. This is realized by adiabatic propagation of wave packets along the corresponding potential energy surface, E_0. We shall restrict our study of torsional dynamics to the region of the valley of the potential energy surface along $\phi=-\psi$ where the barriers to conformational changes are not extremely high. In particular, we consider a transition between the two lowest conformations, i.e., the C_7 and the C_5 minimum. We assume the glycine dipeptide molecule to be initially prepared in the lowest torsional state of either minima. The corresponding zero point energy of the torsional motion is 42 cm^{-1} (C_7) or 26 cm^{-1} (C_5). We assume that the torsional motion of the backbone is instantaneously excited. This energy transfer could be realized in a collision with a solvent molecule, see, e.g., the quantum-classical studies of collisions of a sodium ion[29] or a water molecule with a dipeptide[30] or a small protein.[31] The initial torsional wave packet is given by

$$u_0(q)=N\exp[-ik_0^T q-(q-q_0)^T W(q-q_0)], \qquad (3.4)$$

where N is a normalization constant and W determines the shape of the enveloping two-dimensional Gaussian packets. With uncertainties of $\delta\phi=1/\sqrt{W_{\phi\phi}}=3.5°$ and $\delta\psi=1/\sqrt{W_{\psi\psi}}=5.1°$ for the C_7 minimum or $\delta\phi=6.0°$ and $\delta\psi=6.5°$ for the C_5 minimum (assuming $W_{\phi\psi}=W_{\psi\phi}=0$ throughout), the Gaussian packet provides a good approximation for the stationary torsional states. The direction of the initial torsional momentum, $\hbar k_0$, was chosen along a straight line connecting the initial minimum with the $C_7\leftrightarrow C_5$ saddle. The magnitude of k_0 was varied such that the ''wave packet trajectory,'' i.e., the expectation value, $\langle q\rangle(t)$, connects the initial minimum with the final one, see top part of Fig. 8. This results in momentum vectors with $|k_0|=1.08$ for the $C_7\rightarrow C_5$ transition or $|k_0|=1.05$ for the reversed process (given in reciprocal degrees). The corresponding values of the kinetic energy of 13.9 or 11.3 kJ/mol, respectively, are similar to those considered in previous studies of collisions of solvent particles with a dipeptide.[29,30] Note that these values are almost a factor of two higher than one would anticipate from the energy differences of the minima and the saddle involved, see Table I. The reason for this seeming discrepancy is that the ''trajectories'' for the conformational transitions are not exactly following a minimum energy path due to inertia effects. It is also noted that the two paths are not identical to each other. In addition to the movement of their centers, the wave packets are also subject to strong dispersion. Upon reaching the final conformation, widths of the order of $20\cdots30$ degrees are typically found. For the initial conditions specified here, the change from the C_7 to the C_5 conformation takes 770 fs while the reversed process lasts 740 fs. However, with no dissipative mechanism included in the current simulations, the wave packets are not trapped in the final conformation but rather continue to explore the Ramachandran plane. For a dissipative wave-packet dynamics study of electronically excited molecules, see, e.g., Ref. 53. We have also studied conformational transitions for glycine dipeptide being in an amide I vibrationally excited state by propagating wave packets on potential energy surface obtained as the sum of the electronic energy and either the lower or the upper harmonic amide I excitation energies. Because the latter ones vary by less than 1 kJ/mol$=83.59$ cm^{-1}, they modify the former one only very slightly leading to practically identical wave packet dynamics.

F. Nonadiabatic conformational dynamics

It is very intriguing to study nonadiabatic wave packet dynamics along coupled amide I vibrational states. We choose the two fundamentally excited states exhibiting (avoided) intersections as discussed above. In particular, the question shall be raised how nonadiabatic population transfer

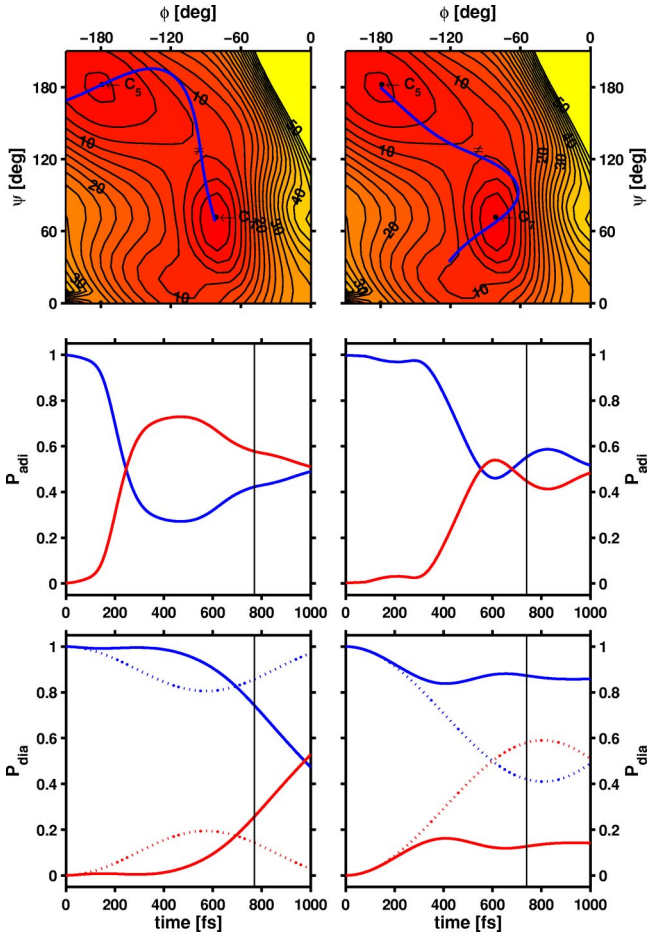

FIG. 8. (Color online) Quantum dynamical picture of $C_7 \rightarrow C_5$ (left) and $C_5 \rightarrow C_7$ (right) conformational changes of glycine dipeptide. Top: Path of the center of the wave packet during the first picosecond. In addition, the ground state adiabatic potential energy surface is shown. Middle: Adiabatic population dynamics, $P_{+,-}(t)$, for an initially prepared delocalized amide I vibration (adiabatic state). Vertical lines indicate the time span until the wave packet center has reached the target state. Bottom: Diabatic population dynamics, $P_{1,2}(t)$, for an initially prepared local amide I vibration (diabatic state). Dotted curves: Population dynamics for stationary torsional states $(k_0=0)$.

can be triggered by a conformational transition. For that purpose we solve the time-dependent Schrödinger equation with Hamiltonian (2.2) for the vector containing the coupled, time-dependent torsional wave functions $(\chi_1(q,t), \chi_2(q,t))$ thus yielding diabatic populations $P_{1,2}(t) = \langle \chi_{1,2}(t) | \chi_{1,2}(t) \rangle$. The corresponding adiabatic dynamics is expressed in terms of populations of the upper $(+)$ and lower $(-)$ state, $P_{+,-}(t) = \langle \chi_{+,-}(t) | \chi_{+,-}(t) \rangle$, which is obtained by transforming the torsional wave functions to the adiabatic representation using the matrix of eigenvectors of the potential energy matrix $V(q)$. We prepare initial wave packets as specified in Eq. (3.4) and promote them to the excited states, where the two coefficients are chosen according to an eigenvector of the diabatic potential energy matrix evaluated at the center of the Gaussian, q_0, i.e., at the C_7 and C_5 minimum of the potential energy surface. The course and shape of the torsional wave packet is essentially the same as in the adiabatic simulations. However, the population dynamics exhibits strongly nonadiabatic behavior, see middle panel of Fig. 8. The $C_7 \rightarrow C_5$ conformational change is indeed accompanied by a significant population transfer. After about 250 fs, the population of the initially unoccupied (lower) adiabatic state exceeds that of the upper state and reaches a maximum of about 70% after 500 fs. Upon reaching the final C_5 conformation after 770 fs, the population of upper and lower state amounts to 42% and 58%, respectively. A similar picture emerges for the $C_5 \rightarrow C_7$ conformational change where the lower state population exceeds that of the upper state after about 550 fs. Populations of 57% and 43% are found for the upper and lower state upon reaching the C_7 conformation after 740 fs. In both cases the rate of nonadiabatic population transfer is determined by the gradient of the mixing angle (2.3). Hence, nonadiabatic effects are most significant at the walls of the trough visible in the lower part of Fig. 5 where the symmetric or antisymmetric character of upper and lower amide I normal mode are changing their role. Because of the clearly distinct infrared intensities of symmetric and anti-symmetric modes (see Fig. 4), it is expected that the strongly nonadiabatic behavior should be detectable by means of transient spectroscopy[6,34] thus allowing an experimental detection of a conformational change.

Another interesting aspect concerns possible mechanisms for energy transfer along the peptide chain. The Davydov model[55] was used to describe the energy transport for protein α helices leading to nonlinear localization of energy.[56,57] In that context it is of interest to study the dependence of the energy flow between neighboring peptide units as a function of the conformational structure and dynamics. Using our two state-two mode Hamiltonian, the time evolution of initially diabatic, i.e., localized amide I vibrational excitations is studied. First consider the situation for a stationary conformational state $(k_0=0)$. Neglecting the widths of the torsional bound states, the population of the initially unoccupied state is given by[58]

$$P_1 = 1 - P_2 = \sin^2(2\alpha)\sin \omega t. \tag{3.5}$$

The amplitude of the oscillations of 19% for C_7 or 62% for C_5 is given by a Rabi-type formula governed by the mixing angles of $-13°$ or $26°$, respectively. The Bohr frequency is given by $\omega = (E_+ - E_-)/\hbar$ where adiabatic energy gaps of 31 cm^{-1} (C_7) or 21 cm^{-1} (C_5) lead to oscillation periods of 1080 or 1530 fs. The population dynamics for the stationary torsional states given by the two-dimensional Gaussian packet (3.4) but with $k_0=0$ are shown in the lower part of Fig. 8 (dotted curves). The finite widths lead to slightly longer oscillation periods for C_7 (1140 fs) and C_5 (1620 fs) while leaving the amplitudes practically unchanged. In passing we note that energy transport between amide I oscillators in a protein occurs on a similar time scale.[57]

In order to explore the effect of torsional dynamics on the coupling of the locally excited amide I vibrational states, we return to the conformational changes characterized above $(k_0 \neq 0)$. Coupled Schrödinger equations are solved for the diabatic Hamiltonian (2.2) with a single diabatic state initially prepared and with the initial momentum chosen as described previously. For the $C_7 \rightarrow C_5$ transition, we find a suppression of the oscillations for the first 400 fs resulting in stabilization of the localized amide I vibrations. Subse-

quently, however, population is rapidly transferred even exceeding 50% at 950 fs. This behavior can be intuitively explained by comparing the path of the isomerization with the Ramachandran plot of the mixing angle (Fig. 5). After starting from C_7, the wave packet is moving through the zero of α where $\sin^2(2\alpha)$ is small. Finally, it passes a region of large positive α before reaching the C_5 conformation. For the $C_5 \rightarrow C_7$ transition, similar reasons lead to a significant reduction of the population transfer. Over the whole duration of the conformational change the initial state does not loose more than 15% of its population. In summary, the energy transfer between neighboring peptide units is strongly influenced by conformational dynamics of the backbone.

IV. CONCLUSIONS

The concept of nonadiabatic quantum dynamics, which has been up to date mainly applied to vibronic effects in small gas phase molecules, is transferred for the first time to vibrational spectroscopy of a peptide systems. A two mode-two state model for the study of amide *I* vibrational dynamics of glycine dipeptide has been presented where the conformational structure and dynamics is modeled in terms of two dihedral angles of the molecular backbone. Potential energy surfaces and harmonic frequencies have been obtained from electronic structure calculations at the DFT [B3LYP/6-31+G(*d*)] level of theory. It has been found that the ordering of the energetically most stable isomers C_7 and C_5 is reversed upon inclusion of the quantum mechanical zero point vibrational energy. In the framework of the vibrationally adiabatic approximation, the torsional surfaces of the two amide *I* excitation frequencies show evidence of (avoided) seams. Hence, quantum dynamical studies of conformational changes using representative wave packets exhibit strongly nonadiabatic behavior with significant transition probabilities between the coupled amide *I* states. Because of the largely different (infrared or Raman) intensities of the two amide excited states there are good prospects for the observation of conformational dynamics in real time. Eventually, this should lead to a fingerprint of such a transition by means of (time-dependent) amide *I* vibrational spectroscopy.[6]

It is tempting to pursue analogous studies of the quantum dynamics of other amide modes of the peptide units. For example, biomolecular conformations were studied by spectroscopy of the amide A modes as well.[52] However, our DFT results of the adiabatic amide A vibrations of glycine dipeptide exhibit an extremely weak coupling between the two NH-stretching modes. Another vibrational mode known for its strong conformational dependence is the amide *III* mode. In our vibrational analysis of glycine dipeptide, we found a strong congestion of the amide *III* modes and out-of-plane bending–twisting of the central CH_2 group thus rendering the reconstruction of diabatic states impossible, too. However, this mixing does not occur for peptides with side chains, see, e.g., the studies of polyalanine.[59,60]

Clearly it will be valuable to extend the present study to conformational structure and dynamics of larger peptide systems where this work should serve as a benchmark. In doing so, the following two aspects need to be considered. The first one concerns the quality of the potential energy surfaces: While the relatively small number of atoms in glycine dipeptide allows to pursue high-level electronic structure calculations yielding reliable potential energy surfaces, it is inevitable to use (semi)empirical force fields for the study of longer peptide chains and proteins. The adequacy of that approach with respect to the prediction of conformations and (free) energy surfaces has been investigated thoroughly, e.g., for trialanine[14] and tetrapeptide.[37] An especially delicate issue is the use of force fields for vibrational spectroscopy of biologically relevant molecules. While standard force fields are known to exhibit major flaws, there are encouraging results for amino acids using modified semiempirical electronic structure theory.[25] The second question pertains to the theoretical description of the conformational dynamics: While the current two mode–two state model of glycine dipeptide allows for a fully quantum mechanical treatment of conformational changes and nonadiabatic transitions between vibrationally excited states, the exponential scaling of the numerical effort of quantum-mechanical calculations renders such an approach unfeasible for systems of much higher complexity. However, the largely different time and energy scales of slow (torsional) and fast (stretching) degrees of freedom suggest a mixed quantum-classical treatment of vibrational modes. In recent work a mean-field (Ehrenfest) quantum-classical approach was used to study the collision of an ion[29] or water[30] with a dipeptide. A more consistent approach to the coupling of quantum and classical subsystem dynamics is given in terms of the quantum-classical Liouville equation[61] for which efficient numerical integrators have recently been devised.[62]

ACKNOWLEDGMENTS

Financial support by the *Deutsche Forschungsgemeinschaft* through program SFB 450 on ''Analysis and control of ultrafast photoinduced reactions'' is gratefully acknowledged. The quantum-chemical calculations were carried out on an IBM pSeries 690 supercomputer available at the HLRN.

[1] S. Krimm and J. Bandekar, Adv. Protein Chem. **38**, 181 (1986).
[2] W. K. Surewicz and H. H. Mantsch, in *Spectroscopic Methods for Determining Protein Structure in Solution*, edited by H. A. Havel (VCH, 1996), pp. 135–162.
[3] A. Barth and C. Zscherp, Q. Rev. Biophys. **35**, 369 (2002), URL http://dx.doi.org/10.1017/S0033583502003815.
[4] P. Hamm, M. Lim, and R. M. Hochstrasser, J. Phys. Chem. B **102**, 6123 (1998), URL http://dx.doi.org/10.1021/jp9813286.
[5] C. Scheurer, A. Piryatinski, and S. Mukamel, J. Am. Chem. Soc. **123**, 3114 (2001), URL http://dx.doi.org/10.1021/ja003412g.
[6] S. Woutersen and P. Hamm, J. Phys.: Condens. Matter **14**, R1035 (2002), URL http://dx.doi.org/10.1088/0953-8984/14/39/202.
[7] A. M. Moran, S.-M. Park, J. Dreyer, and S. Mukamel, J. Chem. Phys. **118**, 3651 (2003), URL http://dx.doi.org/10.1063/1.1538243.
[8] C. Fang, J. Wang, A. K. Charnley, W. Barber-Armstrong, A. B. Smith, III, S. M. Decaturb, and R. M. Hochstrasser, Chem. Phys. **382**, 586 (2003), URL http://dx.doi.org/10.1016/j.cplett.2003.10.111.
[9] E. G. Robertson and J. P. Simons, Phys. Chem. Chem. Phys. **3**, 1 (2001), URL http://dx.doi.org/10.1039/b008225m.
[10] B. C. Dian, A. Longarte, S. Mercier, D. A. Evans, D. J. Wales, and T. S. Zwier, J. Chem. Phys. **117**, 10688 (2002), URL http://dx.doi.org/10.1063/1.1521132.
[11] J. M. Bakker, L. M. Aleese, G. Meijer, and G. von Helden, Phys. Rev.

Lett. **91**, 203003 (2003), URL http://dx.doi.org/10.1103/PhysRevLett.91.203003
[12] S. Woutersen, Y. G. Mu, G. Stock, and P. Hamm, Proc. Natl. Acad. Sci. U.S.A. **98**, 11254 (2001), URL http://dx.doi.org/10.1073/pnas.201169498
[13] K. Kwac and M. Cho, J. Chem. Phys. **119**, 2256 (2003), URL http://dx.doi.org/10.1063/1.1580808
[14] Y. Mu, D. S. Kosov, and G. Stock, J. Phys. Chem. B **107**, 5064 (2003), URL http://dx.doi.org/10.1021/jp022445a
[15] J. Bredenbeck, J. Helbing, R. Behrendt, C. Renner, L. Moroder, J. Wachtveitl, and P. Hamm, J. Phys. Chem. B **107**, 8654 (2003), URL http://dx.doi.org/10.1021/jp034552q
[16] B. C. Dian, A. Longarte, P. R. Winter, and T. S. Zwier, J. Chem. Phys. **120**, 133 (2004), URL http://dx.doi.org/10.1063/1.1626540.
[17] B. C. Dian, J. R. Clarkson, and T. S. Zwier, Science **303**, 1169 (2004), URL http://dx.doi.org/10.1126/science.1093731.
[18] H. Torii and M. Tasumi, J. Raman Spectrosc. **29**, 81 (1998), URL http://dx.doi.org/10.1002/(SICI)1097-4555(199801)29:1⟨81::AID-JRS214⟩3.0.CO2-H.
[19] S. Cha, S. Ham, and M. Cho, J. Chem. Phys. **117**, 740 (2002), URL http://dx.doi.org/10.1063/1.1483257.
[20] S. Ham and M. Cho, J. Chem. Phys. **118**, 6915 (2003), URL http://dx.doi.org/10.1063/1.1559681.
[21] S. Ham, S. Cha, J.-H. Choi, and M. Cho, J. Chem. Phys. **119**, 1451 (2003), URL http://dx.doi.org/10.1063/1.1581855.
[22] S. K. Gregurick, G. M. Chaban, and R. B. Gerber, J. Phys. Chem. A **106**, 8696 (2002), URL http://dx.doi.org/10.1021/jp025633+.
[23] S. Woutersen and P. Hamm, Bull. Chem. Soc. Jpn. **75**, 985 (2002), URL http://dx.doi.org/10.1246/bcsj.75.985.
[24] T. M. Watson and J. D. Hirst, Phys. Chem. Chem. Phys. **6**, 998 (2004), URL http://dx.doi.org/10.1039/b312181j.
[25] B. Brauer, G. M. Chaban, and R. B. Gerber, Phys. Chem. Chem. Phys. **6**, 2543 (2004), URL http://dx.doi.org/10.1039/b315326f.
[26] A. E. Roitberg, R. B. Gerber, and M. A. Ratner, J. Phys. Chem. B **101**, 1700 (1997), URL http://dx.doi.org/10.1021/jp9629194.
[27] D. C. Clary, J. Chem. Phys. **114**, 9725 (2001), URL http://dx.doi.org/10.1063/1.1368402.
[28] P. H. Nguyen and G. Stock, J. Chem. Phys. **119**, 11350 (2003), URL http://dx.doi.org/10.1063/1.1622654.
[29] M. L. Wang and J. Z. H. Zhang, J. Chem. Phys. **118**, 7846 (2003), URL http://dx.doi.org/10.1063/1.1563610.
[30] M. L. Wang and J. Z. H. Zhang, J. Chem. Phys. **119**, 11152 (2003), URL http://dx.doi.org/10.1063/1.1622666.
[31] D. C. Clary and A. J. H. M. Meijer, J. Chem. Phys. **116**, 9829 (2002), URL http://dx.doi.org/10.1063/1.1476319.
[32] H. Goldstein, *Classical Mechanics* (Addison-Wesley, Reading, Ma., 1950).
[33] V. I. Arnold, V. V. Kozlov, and A. I. Neishtadt, *Mathematical Aspects of Classical and Celestial Mechanics* (Springer, Berlin, 1997).
[34] W. Domcke and G. Stock, Adv. Chem. Phys. **100**, 1 (1997).
[35] *Conical Intersections. Electronic Structure, Dynamics and Spectroscopy, Vol. 15 of Advanced Series in Physical Chemistry*, edited by W. Domcke, D. R. Yarkony, and H. Köppel (World Scientific, Singapore, 2004).
[36] T. Head-Gordon, M. Head-Gordon, M. J. Frisch, C. L. Brooks, III, and J. A. Pople, J. Am. Chem. Soc. **113**, 5989 (1991).
[37] M. D. Beachy, D. Chasman, R. B. Murphy, T. A. Halgren, and R. A. Friesner, J. Am. Chem. Soc. **119**, 5908 (1997), URL http://dx.doi.org/10.1021/ja962310g.
[38] G. Cuevas, V. Renugopalakrishnan, G. Madrid, and A. T. Hagler, Phys. Chem. Chem. Phys. **4**, 1490 (2002), URL http://dx.doi.org/10.1039/b110777c.
[39] A. Perczel, Ö. Farkas, I. Jakli, I. A. Topol, and I. G. Csizmadia, J. Comput. Chem. **24**, 1026 (2003), URL http://dx.doi.org/10.1002/jcc.10267.
[40] C. Ramakrishnan and G. N. Ramachandran, Biophys. J. **5**, 909 (1965).
[41] Tech. Rep., IUPAC–IUB (1969), URL http://www.chem.qmul.ac.uk/iupac/misc/ppep1.html
[42] *Special Issue: Progress in Density Functional Theory*, J. Comput. Chem. **20**, 1 (1999), URL http://dx.doi.org/10.1002/(SICI)1096-987X(19990115)20:1<V::AID-JCC1>3.0.CO;2-W
[43] M. J. Frisch, G. W. Trucks, H. B. Schlegel *et al.*, GAUSSIAN 98, Revision A.7, Gaussian, Inc., Pittsburgh, PA, 1998.
[44] R. Meyer and H. H. Günthard, J. Chem. Phys. **50**, 353 (1969), URL http://dx.doi.org/10.1063/1.1670803.
[45] R. Meyer and E. B. Wilson Jr., J. Chem. Phys. **53**, 3969 (1970), URL http://dx.doi.org/10.1063/1.1673867.
[46] J. E. Hadder and J. H. Frederick, J. Chem. Phys. **97**, 3500 (1992), URL http://dx.doi.org/10.1063/1.462985.
[47] H. Köppel, J. Gronki, and S. Mahapatra, J. Chem. Phys. **115**, 2377 (2001), URL http://dx.doi.org/10.1063/1.1383986.
[48] R. Kosloff, Annu. Rev. Phys. Chem. **45**, 145 (1994), URL http://dx.doi.org/10.1146/annurev.pc.45.100194.001045.
[49] R. Kosloff and H. Tal-Ezer, Chem. Phys. Lett. **127**, 223 (1986), URL http://dx.doi.org/10.1016/0009-2614(86)80262-7.
[50] M. D. Feit, J. A. Fleck, Jr, and A. Steiger, J. Comput. Phys. **47**, 412 (1982).
[51] J. Alvarellos and H. Metiu, J. Chem. Phys. **88**, 4957 (1988), URL http://dx.doi.org/10.1063/1.454707.
[52] I. V. Rubtsov, J. Wang, and R. M. Hochstrasser, J. Chem. Phys. **118**, 7733 (2003), URL http://dx.doi.org/10.1063/1.1570398.
[53] B. Balzer, S. Hahn, and G. Stock, Chem. Phys. Lett. **379**, 351 (2003), URL http://dx.doi.org/10.1016/j.cplett.2003.08.052.
[54] Y.-Y. Chuang and D. G. Truhlar, J. Chem. Phys. **112**, 1221 (2000), URL http://dx.doi.org/10.1063/1.480768.
[55] A. S. Davydov, *Solitons in Molecular Systems* (Kluwer Academic, Dordrecht, 1991).
[56] J. Edler, P. Hamm, and A. C. Scott, Phys. Rev. Lett. **88**, 067403 (2002), URL http://dx.doi.org/10.1103/PhysRevLett.88.067403.
[57] D. M. Leitner, J. Phys. Chem. A **106**, 10870 (2002), URL http://dx.doi.org/10.1021/jp0206119.
[58] J. I. Steinfeld, *Molecules and Radiation* (MIT Press, Cambridge, MA, 1985).
[59] R. Schweitzer-Stenner, F. Eker, Q. Huang, K. Griebenow, P. A. Mroz, and P. M. Kozlowski, J. Phys. Chem. B **106**, 4294 (2002), URL http://dx.doi.org/10.1021/jp0137118.
[60] N. G. Mirkin and S. Krimm, J. Phys. Chem. A **106**, 3391 (2002), URL http://dx.doi.org/10.1021/jp012324v.
[61] R. Kapral and G. Ciccotti, J. Chem. Phys. **110**, 8919 (1999), URL http://dx.doi.org/10.1063/1.478811.
[62] I. Horenko, M. Weiser, B. Schmidt, and C. Schütte, J. Chem. Phys. **120**, 8913 (2004), URL http://dx.doi.org/10.1063/1.1691015.